Dynamics within a tunable harmonic plus quartic waveguide

Rudolph N. Kohn, Jr. ⬡[*] and James A. Stickney ⬡

Space Dynamics Laboratory, Albuquerque, New Mexico 87106, USA

We present a method for measuring nonharmonic contributions to the trapping potential of a cold atomic gas by measuring the dynamics of the cloud. This method can be used to minimize the anharmonicity of a trap, or to tune the quartic anharmonicity to some desired level in a sufficiently tunable trap. We present an approximate solution to the dynamics of a classical noninteracting cloud of thermal atoms in a cigar-shaped harmonic trap with a quartic perturbation along the weakly confined axis which is analytical and closed form. We calculate the first and second moments of position along the weak axis as functions of time, which is sufficient to characterize the trap. The dynamics of the thermal cloud differ notably from those of a single particle, with an offset to the oscillation frequency that persists even as the oscillation amplitude approaches zero. We also present some numerical results that describe the effects of time of flight on the behavior of the cloud in order to better understand the results of a hypothetical experimental realization of this system.

I. INTRODUCTION

Cold atom interferometers have proven themselves invaluable tools for examining a variety of phenomena by leveraging the wave nature and large rest mass of atoms to make extremely precise measurements. They have been used to measure gravity [1–4], multiaxis accelerations [5–7], rotations [8–10], electric polarizability [11], fundamental quantities such as the fine structure constant [12], and to test predictions of general relativity [13]. Typically, free space atom interferometers use controlled light pulses to apply coherent momentum kicks to separate clouds into subsets with different momenta and reflect them back toward each other. Between kicks, the atoms evolve in free space. Acceleration due to gravity limits the sensitivity of these devices, because the vacuum chamber must grow with the square of the interrogation time.

This limitation can be overcome by supporting the atomic gas against gravity using external potentials. As a result, interferometers using trapped atoms can be smaller than their free space counterparts. The potentials typically have a preferred axis which makes precise alignment of the excitation beams critical [8]. In addition, if the trapped atomic cloud is reflected with a laser pulse, both mean-field pressure and residual curvature reduce the visibility of the interference fringes [8,9,11,14]. One promising method for overcoming these limitations is to allow the atoms to complete a full oscillation in the confinement potential [15,16].

Using the potential to reflect the clouds means that, for a given separation, the interrogation time can be longer. However, uncontrolled variation in the trap potential and induced excitations can cause unwanted loss of interference contrast

[15]. Mean-field effects can be mitigated by reducing the atomic density. However, any realistic trapping potential will depart somewhat from the desired shape, if only because of errors introduced in the fabrication process. Therefore, it is extremely valuable to be able to identify and compensate for unwanted deviations in the trap shape, especially if it can be done without altering the hardware.

In a previous work [17], we developed a method for producing atom chip traps with a potential that tightly confines the atoms in two dimensions and enables fine control of the potential along the third, weakly confined direction. This is carried out by tuning currents in several parallel wires. The spacing of the wires can be chosen to minimize higher order contributions. These tunable atom chip traps can generate carefully tailored potentials, including tuning out imperfections caused by the manufacturing process.

To enable these adjustments, a method for gauging the undesirable contributions to the potential is crucial. We will show that this can be accomplished by measuring the dynamics of a trapped thermal atomic cloud, and comparing them to a theoretical model. The primary goal of this paper is the presentation of such a model. Of note is that comparison to the model also provides an estimate to the quartic contribution to the trap, which can be useful if a certain amount of anharmonicity is desired for an experiment.

To this end, we examine the dynamics of a cold but classical cloud of atoms in a one-dimensional trap with harmonic and quartic components. It will be assumed that the other two axes are well confined and separable. The harmonic and quartic terms are particularly interesting because the harmonic term is solvable and the quartic term is often the leading unwanted contribution in trapped atom interferometers [15]. The solution described here may also see utility in experiments that create multiple potential wells, as in Berrada *et al.* [18], as the resulting traps may have significant anharmonic contributions. Optomechanics experiments have also

_____
[*]rudy.kohn@sdl.usu.edu

dealt with anharmonic contributions, which affect the behavior of the trapped particle with some similarities, such as frequency shifts, compared to what we will show below [19–21]. With a few minor approximations, we will derive analytical, closed-form solutions for the behavior of single particles and ensembles and show that there are qualitative differences between them.

The purely harmonic case can be thoroughly described using Boltzmann's kinetic theory. One of the more counterintuitive results of that theory involves the behavior of the cloud at long times. While it might be assumed that a system of atoms in a perfectly harmonic trap would eventually reach some kind of thermal equilibrium, certain excitation modes, such as the monopole breathing mode, actually persist indefinitely, even in the presence of isotropic, energy-independent, elastic collisions. In fact, it can be shown that for the dynamical quantities that describe a monopole breathing mode in a perfectly harmonic trap, the collisional integral is exactly zero, and the oscillations persist indefinitely [22]. In contrast, the dynamical quantities which describe a quadrupole oscillation do not satisfy the requirements for a zero collisional integral, and such oscillations damp out on the collisional time scale. The persistence of the monopole breathing mode and decay of quadrupole motion were demonstrated experimentally in a system of cold atoms by Lobser *et al.* [23] in 2015.

Some simple substitutions show that, in addition to monopole breathing, center-of-mass oscillations of a small cloud along the weak axis of a cylindrically symmetric harmonic trap will also persist indefinitely, so long as the axes are separable, and collisions are isotropic, elastic, and energy independent [22]. We will show below that the dynamical quantities involved in such oscillations are similarly undamped. We will refer to this particular type of motion, which resembles a small amount of liquid moving back and forth in a bowl after shaking it, as "sloshing." As we will show, the addition of a quartic perturbation has several effects. Most importantly, the quartic perturbation causes initially close atoms with slightly different energies to gradually separate, effectively randomizing their polar angles in phase space and resulting in the gradual decay of sloshing and the spreading out of the cloud in an equilibriumlike state at the center of the trap, even in the absence of collisions. The time scale for this apparent equilibration is unrelated to the collision rate and can be used to characterize the anharmonic contributions to the trapping potential. In a real world application for sensing, the cloud would be prepared in a low collision regime anyway [24], but even if collisions have a effect on the damping of sloshing motion, that motion can be effectively damped much more quickly by the phase shifts between atoms with different energies, although this apparent equilibrium is different from thermalization in the sense that it is deterministic and therefore may be reversible to some degree.

In one of our tunable atom chip traps, the parameters can be adjusted to minimize this apparent equilibration and iteratively approach a perfectly harmonic potential. If the trap is designed to minimize higher order terms, the quartic contribution can be tuned to some desired value as well. In addition, we will see below that the quartic contribution alters the frequency of the trap for clouds of atoms, even at infinitesimally small sloshing amplitudes. Finally, the use of

two independent parameters to describe our traps necessitates the measurement of two independent characteristics of the cloud. The first two moments of position, $\langle x \rangle$ and $\langle x^2 \rangle$, serve this purpose. In practice, the center-of-mass position and size of the cloud are easily measured and can be expressed in terms of these two moments.

This paper is divided into several sections. In Sec. II, we will proceed through the analytical solution of the one-dimensional harmonic plus quartic trap. Section III describes the results of the theory and examines some of the finer details. In Sec. IV, we use numerical methods to calculate the behavior of the clouds after some time of flight. In an experimental realization of this system, it is likely that time of flight will be used to more easily image the atoms. Therefore, some basic understanding of the behavior of the cloud after time of flight will show how various parameters are qualitatively expected to change, and will show that the general form of the solution is still applicable. Finally, we will summarize our conclusions and describe some future paths for inquiry in Sec. V.

II. THEORY

To start, we review some results from Guéry-Odelin *et al.* [22] and apply them to our system. In a cigar-shaped harmonic trap, the potential energy is

$$U = \frac{m\omega^2}{2}x^2 + \frac{m\omega_\perp^2}{2}(y^2 + z^2). \tag{1}$$

The expectation values of certain dynamical quantities χ are

$$\frac{d\langle \chi \rangle}{dt} - \langle \boldsymbol{v} \cdot \boldsymbol{\nabla}_r \chi \rangle - \left\langle \frac{-\boldsymbol{\nabla}_r U}{m} \cdot \boldsymbol{\nabla}_v \chi \right\rangle = \langle \chi I_{\text{coll}} \rangle. \tag{2}$$

The value of the collisional integral, $\langle \chi I_{\text{coll}} \rangle$, is zero as long as

$$\chi = a(\boldsymbol{r}) + \boldsymbol{b}(\boldsymbol{r}) \cdot \boldsymbol{v} + c(\boldsymbol{r})v^2. \tag{3}$$

This is because values of χ that satisfy Eq. (3) are unchanged by elastic, isotropic, energy-independent collisions [22]. By calculating Eq. (2) for a few different values of χ, we find solutions for the dynamics of $\langle x \rangle$ and $\langle x^2 \rangle$ which are independent of the behavior in the other two axes and have the form,

$$\langle x \rangle \propto \text{Re}(\exp(i\omega t + \phi)) \text{ and } \langle x^2 \rangle \propto \text{Re}(\exp(2i\omega t + 2\phi)), \tag{4}$$

where ϕ is some angle to match initial conditions. Thus, the dynamics in the weak axis of the purely harmonic cigar-shaped trap resemble sloshing as described above: A small cloud oscillates periodically in the trap, with its size oscillating at twice that frequency. Neither oscillation is damped in the harmonic case. The other two axes exhibit similar oscillatory motion, with the frequency $\omega_\perp$ substituted for ω.

We will assume going forward that the motion of the atomic gas in the x direction can be decoupled from the motion in the y and z directions, i.e., $H_t = H(x, p_x) + H_\perp(y, z, p_y, p_z)$. We now add the perturbation along the x axis, leaving it mostly harmonic, with a small quartic term. Thus, the Hamiltonian,

$$H = \frac{p^2}{2m} + m\omega^2 \left(\frac{x^2}{2} + \frac{x^4}{4x_4^2} \right), \tag{5}$$

governs the dynamics, with m as the atomic mass, ω as the harmonic trap frequency, and x_4 describing the quartic contribution. We have also used p as shorthand for p_x and will continue to do so going forward. The magnitude of x_4 corresponds to the value of x for which the forces due to the harmonic and quartic terms are equal. However, to allow for both postive and negative quartic contributions, x_4^2 can be either positive or negative, corresponding to purely real or purely imaginary values for x_4.

In the limit where the oscillation amplitude A is small, i.e., $A \ll |x_4|$, the dynamics of a particle in the Hamiltonian given by Eq. (5) can be approximated by a sinusoid with an amplitude-dependent frequency. The position of the particle is approximately

$$\frac{x(t)}{A} = \cos(\Omega t - \phi_0) + \frac{1}{32}\frac{A^2}{x_4^2}\cos(3\Omega t - 3\phi_0), \quad (6)$$

where A is the amplitude and ϕ_0 is the initial polar angle of the particle in phase space. The amplitude-dependent frequency is

$$\frac{\Omega}{\omega} = 1 + \frac{3}{8}\frac{A^2}{x_4^2}, \quad (7)$$

and does not depend on ϕ_0. We neglect the part of the dynamics which oscillates at the frequency 3Ω in later calculations because its magnitude is small compared to the Ω term. We note that this approximation does result in a deviation from conservation of energy for a single particle. This deviation is oscillatory and scales as A/x_4^2. Since $A \ll x_4$ is already a requirement of the approximation, this quantity will be small. For a system with $A = 2.8$, $\omega = 100$ and $x_4 = 8$, the peak-to-peak energy variation divided by the average energy is about 3.4%.

Since the real world application will likely involve very cold, trapped atoms, we estimated the magnitude of quantum effects and find that they can be neglected so long as

$$\frac{\hbar^2}{mx_4^2k_BT} \ll 1. \quad (8)$$

For a realistic implementation, e.g., $T = 10^{-7}$ K, $m = 1.44 \times 10^{-25}$ kg, and $x_4 = 1$ mm, the relevant quantity is less than 10^{-7}. We also estimated mean-field effects, and they will be negligible as long as

$$\frac{\hbar^2 a_s \omega_\perp^2}{(k_BT)^2\sigma_x} \ll 1, \quad (9)$$

where a_s is the scattering length of the particle and $\omega_\perp$ is the frequency of oscillation in the unperturbed axes, as used in Eq. (1). In a realistic implementation, e.g., $\sigma_x = 10^{-5}$ m, $a_s = 100a_0$ (where a_0 is the Bohr radius and a_s here is comparable to ^{87}Rb's scattering length), $T = 10^{-7}$ K, and $\omega_\perp = 10^3$ s^{-1}, this is about 3×10^{-4}. Therefore we also neglect mean-field effects.

The effect of the perturbation on the dynamics of a single particle becomes dependent on only the amplitude of oscillation. It is convenient to recast this in terms of the unperturbed energy,

$$E \equiv \frac{p_0^2}{2m} + \frac{1}{2}m\omega^2x_0^2, \quad (10)$$

where x_0 and p_0 are the initial position and momentum.

Using the unperturbed energy and the other composite variables described above, we can describe the dynamics of a single particle as

$$x(t) = \sqrt{\frac{2E}{m\omega^2}}\cos(\Omega t - \phi_0), \quad (11)$$

where $\tan\phi_0 = p_0/m\omega x_0$ and

$$\frac{\Omega}{\omega} = 1 + \frac{3}{8}\frac{2E}{m\omega^2x_4^2}. \quad (12)$$

In short, a particle sloshes back and forth in the perturbed potential, and its frequency depends on its energy. However, the sloshing of a small cloud will be shown to have some specific quantitative differences from a single particle, even in the limit of small oscillation amplitude. From these expressions, we see that any particle can be placed on a closed ellipse in phase space and traces out that ellipse with a frequency that depends only on energy. Figure 1 illustrates this effect by plotting the phase space distribution of a cloud in a harmonic plus quartic trap at several different times.

A classical cloud of atoms can be described by its phase space density $f(x, p, t)$. The nth moment of position of the cloud is

$$\langle x^n \rangle = \int_{-\infty}^{\infty}\int_{-\infty}^{\infty}dxdp\, x^n f(x, p, t). \quad (13)$$

In general, the phase space density $f(x, p, t)$ evolves in time, but in a noninteracting, conservative system each element of phase space moves independently from all others. The stationary and comoving frames are identical at $t = 0$ but not at other values of t. If functions that transform between the stationary and comoving frames are $X(x, p, t)$ and $P(x, p, t)$, then we define $X(x, p, -t) = x_R$ and $P(x, p, -t) = p_R$, with x_R and p_R representing the point in phase space at $t = 0$ which corresponds to (x, p) at time t. We can write

$$f(x, p, t) = f(X(x, p, -t), P(x, p, -t), 0)$$
$$= f(x_R, p_R, 0) = f_0(x_R, p_R), \quad (14)$$

where $f_0(x, p) = f(x, p, 0)$ is time independent. Then, this change of variables applied to Eq. (13) leads to

$$\langle x^n \rangle = \int_{-\infty}^{\infty}\int_{-\infty}^{\infty}dxdp\, x_R^n\, f_0(x, p), \quad (15)$$

where the time dependence is now implicitly part of x_R and the phase space density is time independent.

In a real world implementation of a system like this, a cold atom ensemble would be prepared by evaporatively cooling a large cloud of atoms in a tight magnetic trap. This is required to increase the thermalization rate and cool efficiently. The resulting cloud is thermal. After cooling, the atoms are adiabatically transferred into a weaker trap with a relatively low collision rate. As a result, it will be assumed the initial state of the atomic ensemble is given by a thermal distribution in the purely harmonic trap, with temperature T.

For a thermal distribution, the relation between position and momentum is known and it is convenient to transform Eq. (15) into a polar coordinate system such that

$$x = \sqrt{2\xi}\sigma_x\cos\phi \text{ and } p = \sqrt{2\xi}\sigma_p\sin\phi, \quad (16)$$
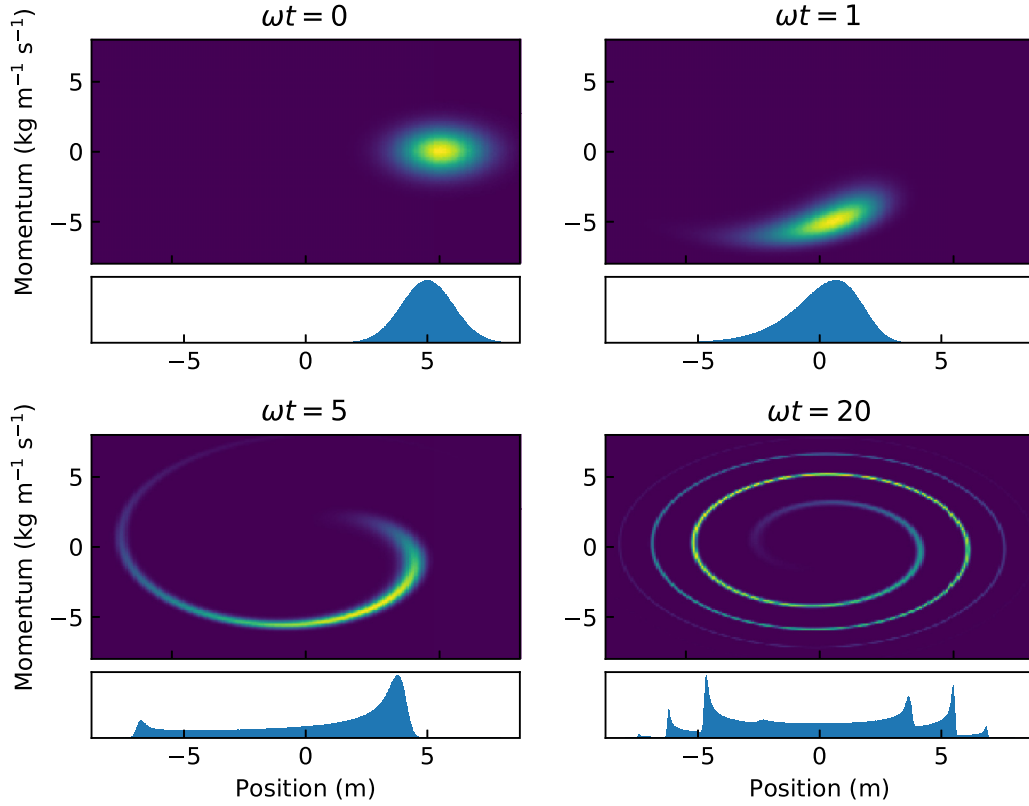
FIG. 1. An illustration showing how an energy-dependent frequency shift results in a gradual approach to pseudoequilibrium, even in the absence of collisions. An initial cloud is produced with parameters $m = 1\,\text{kg}$, $\omega = 1\,\text{s}^{-1}$, $x_4^2 = 20\,\text{m}^2$, $x_D = 5\,\text{m}$, $p_D = 0\,\text{kg m}^{-1}\,\text{s}^{-1}$, and $\sigma_x = \sigma_p = 1.5\,\text{m}$. These values are chosen for their compactness and simplicity and not to resemble any realistically achievable system. We allow the cloud to evolve, and snapshots are taken at several times to illustrate the gradual spreading out of the cloud. The particular times illustrated are chosen because they have the center of mass of the cloud near the center of the trap, so that the spreading out of the cloud in space over time is clearly visible. Additionally shown is a phase-space diagram for each point in time showing how the clean 2D Gaussian at $t = 0$ becomes an increasingly long spiral, as atoms with different energies accumulate relative angles in phase space so that atoms that started near each other with different energies drift apart.

where $\xi = E/k_B T$ is the ratio between phase space energy, Eq. (10), and thermal energy $k_B T$. Both position and momentum are scaled by the thermal standard deviations,

$$\sigma_p = \sqrt{mk_B T} \quad \text{and} \quad \sigma_x = \sqrt{k_B T/m\omega^2}, \qquad (17)$$

to make them unitless. The angle $\tan(\phi) = \sigma_x p/\sigma_p x$ is the initial polar angle of some point (x, p) at $t = 0$. In this new coordinate system,

$$x_R = \sqrt{2\xi}\sigma_x \cos(\Omega t + \phi), \qquad (18)$$

and Eq. (15) becomes

$$\frac{\langle x^n \rangle}{(\sqrt{2}\sigma_x)^n} = \int_0^\infty \int_0^{2\pi} d\xi\, d\phi\, \sigma_x \sigma_p \xi^{n/2} \cos^n(\Omega t + \phi) f_0(\xi, \phi), \tag{19}$$

where $f_0(\xi, \phi)$ is simply the initial phase space density distribution converted to the new coordinate basis.

At the initial time, the atoms are given a kick that affects each atom equally, changing their positions and momenta. This can be accomplished in a variety of ways, for example, by adding a short gradient to the potential. After the kick the mean momentum and position are

$$p_D = \sqrt{2\xi_D}\sigma_p \sin\phi_D \quad \text{and} \quad x_D = \sqrt{2\xi_D}\sigma_x \cos\phi_D. \quad (20)$$

ξ_D and ϕ_D are defined with respect to x_D and p_D in the same way that ξ and ϕ are defined in terms of x and p, such that

$$\xi_D = \frac{x_D^2}{2\sigma_x^2} + \frac{p_D^2}{2\sigma_p^2} \quad \text{and} \quad \tan(\phi_D) = \sigma_x p_D/\sigma_p x_D. \quad (21)$$

We assume that the kick results in a maximum phase-space displacement much larger than the thermal width of the cloud, such that

$$\sqrt{2\xi_D} > 1, \qquad (22)$$

and the maximum displacement in position is much less than x_4. Such a kick will cause the cloud to slosh in the trap.

Using the above conditions, the initial distribution will be

$$f_0(\xi, \phi) = \frac{1}{2\pi \sigma_x \sigma_p} \exp(-\xi - \xi_D + 2\sqrt{\xi \xi_D} \cos(\phi - \phi_D)). \tag{23}$$

Substituting Eq. (23) into Eq. (19) and converting the integral to the new coordinate system yields

$$\frac{\langle x^n \rangle}{(\sqrt{2}\sigma_x)^n} = \frac{e^{-\xi_D}}{2\pi} \int_0^\infty d\xi \xi^{n/2} e^{-\xi} \int_0^{2\pi} d\phi \cos^n(\Omega t + \phi_D + \phi)$$
$$\times \exp(2\sqrt{\xi\xi_D}\cos\phi). \tag{24}$$

The trigonometric power law reduction formula, $\cos^n\theta = \sum_m c_{nm}\cos m\theta$, permits further simplification. Analytic expressions for the coefficients c_{nm} can be found in Gradshteyn and Ryzhik [25], on page 31. In this case, the three elements of interest are $c_{11} = 1$, $c_{20} = 1/2$, and $c_{22} = 1/2$.

Perhaps surprisingly, Eq. (24) can be solved analytically without further approximation. To simplify the notation, the moments can be rewritten as

$$\frac{\langle x^n \rangle}{(\sqrt{2}\sigma_x)^n} = \frac{1}{2}\sum_m c_{nm}(\Upsilon_{nm} + \text{c.c.}), \tag{25}$$

with the Υ_{nm} given as

$$\Upsilon_{nm} = e^{-\xi_D + im(\omega t + \phi_D)} \int_0^\infty d\xi \xi^{n/2}$$
$$\times \exp[-(1 - im\Lambda t)\xi]I_m(2\sqrt{\xi\xi_D}), \tag{26}$$

where $\Lambda \equiv 3\omega\sigma_x^2/8x_4^2$ and I_m is the modified Bessel function of the first kind. The integrals in Υ_{20}, Υ_{11}, and Υ_{22} must be solved to calculate closed-form expressions for $\langle x \rangle$ and $\langle x^2 \rangle$. Υ_{11} and Υ_{22} can be solved in terms of Gradshteyn and Ryzhik [25], section 6.631, equation 4. Υ_{20} can be solved in terms of Gradshteyn and Ryzhik [25], section 6.631, equation 1. The results are

$$\Upsilon_{20} = 1 + \xi_D, \tag{27}$$

$$\Upsilon_{11} = \frac{\sqrt{\xi_D}}{(1 - i\Lambda t)^2}\exp\left[-\xi_D + \frac{\xi_D}{(1 - i\Lambda t)} + i(\omega t + \phi_D)\right], \tag{28}$$

and

$$\Upsilon_{22} = \frac{\xi_D}{(1 - 2i\Lambda t)^3}\exp\left[-\xi_D + \frac{\xi_D}{(1 - 2i\Lambda t)} + i(2\omega t + 2\phi_D)\right]. \tag{29}$$

With these solutions, it is possible to calculate the center-of-mass position and effective size of the cloud as a function of time for any chosen set of parameters that satisfies the approximation requirements described above.

III. RESULTS

Having calculated the values of Υ_{nm}, we can combine them into expressions for the first two moments of position. The first moment is the center-of-mass position of the cloud. The first and second moments together can be used to calculate the effective size of the cloud. The center-of-mass position and size of the cloud are, in general, easily observed and calculated from absorption images in a cold atom realization of this system.
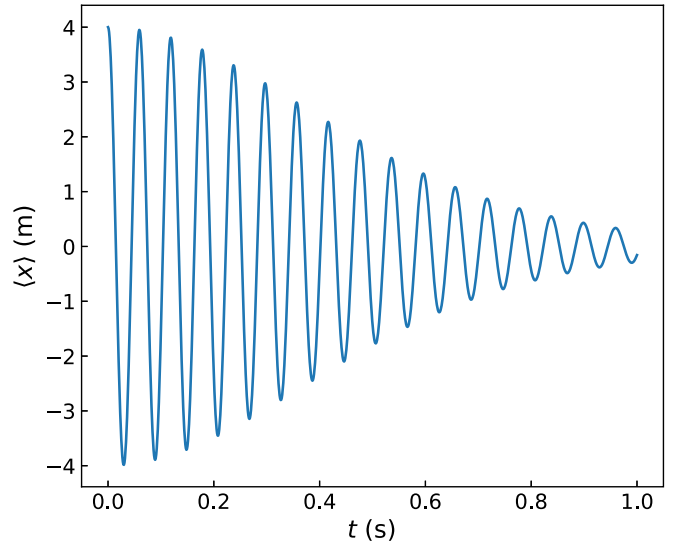

FIG. 2. $\langle x \rangle$ as a function of time. Most of the decay to quasithermal equilibrium is shown. The plot uses parameters $\xi_D = 8$, $\phi_D = 0$, $\omega = 100\ \text{s}^{-1}$, $\sigma_x(t = 0) = 1\ \text{m}$, and $x_4 = 8\ \text{m}$. For these parameters, $\Lambda \cong 0.586$.

Υ_{11} leads to the center-of-mass position of the atomic cloud as a function of time.

$$\langle x \rangle = \frac{\sigma_x\sqrt{2\xi_D}}{[1 + (\Lambda t)^2]^2}\exp\left[\frac{-(\Lambda t)^2\xi_D}{1 + (\Lambda t)^2}\right](\cos(\Phi_1)$$
$$- 2\Lambda t\sin(\Phi_1) - (\Lambda t)^2\cos(\Phi_1)), \tag{30}$$

where $\Phi_1 = \omega t + \phi_D + \Lambda t\xi_D/(1 + (\Lambda t)^2)$. The first moment resembles a decaying sinusoid. The initial decay is Gaussian, but at later times the denominator of the first term takes over. An example of the behavior of the first moment as a function of time appears in Fig. 2. Υ_{20} and Υ_{22} combine to give the second moment,

$$\langle x^2 \rangle = \sigma_x^2(1 + \xi_D) + \frac{\sigma_x^2\xi_D}{[1 + (2\Lambda t)^2]^3}\exp\left[\frac{-(2\Lambda t)^2\xi_D}{1 + (2\Lambda t)^2}\right]$$
$$\times(\cos(\Phi_2) - 6\Lambda t\sin(\Phi_2) - 12(\Lambda t)^2\cos(\Phi_2)$$
$$+ 8(\Lambda t)^3\sin(\Phi_2)), \tag{31}$$

where $\Phi_2 = 2\omega t + 2\phi_D + 2\Lambda t\xi_D/(1 + (2\Lambda t)^2)$. This has a similar form to $\langle x \rangle$, but it oscillates about twice as rapidly, and decays faster as well, as seen in Fig. 3. In fact, the second moment is less illustrative of the dynamics than the size of the cloud as a function of time because the position and size of the cloud are more directly measurable. The standard deviation of the cloud's position distribution is $\sigma_x(t) = \sqrt{\langle x^2 \rangle - \langle x \rangle^2}$ and an example is shown in Fig. 4. Examination of Figs. 2 and 4 shows why we refer to the motion as sloshing: The atoms move back and forth along the weak axis of the trap and the size of the cloud oscillates at about twice the frequency. The decay rates are indicators of the anharmonicity of the trap, and in an experimental realization, adjusting the trap parameters to minimize the decay rate leads toward a maximally harmonic trap. The center-of-mass oscillations gradually decay to zero,
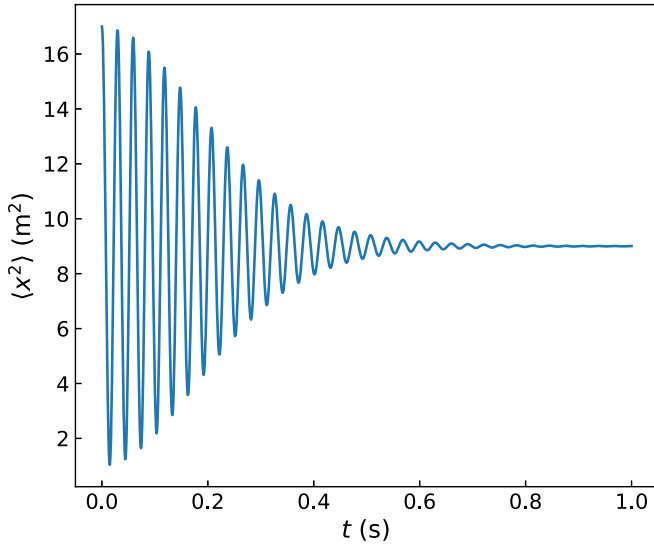
FIG. 3. $\langle x^2 \rangle$ as a function of time for the same parameters as used in Fig. 2. Note the more rapid oscillations as well as the more rapid decay of the oscillations.

and the size of the cloud increases as it oscillates, eventually approaching an asymptotic maximum. As discussed previously, this model does not take collisions into account, so the apparent equilibration is purely a result of the relative motion of parts of the cloud with different energies.

Recalling the issue with the single-particle conservation of energy, we examined the energy of a cloud described by these equations. The majority of the energy deviation is oscillatory, so that as the particles' polar angles in phase space spread out, much of that deviation cancels out. An analytical estimation of the energy of a cloud at $t = 0$ compared to $t \rightarrow +\infty$, assuming that the energy of the cloud as $t \rightarrow +\infty$ was the same as a thermal cloud with identical values for $\langle x(t) \rangle$ and $\sigma_x(t)$, showed two deviation
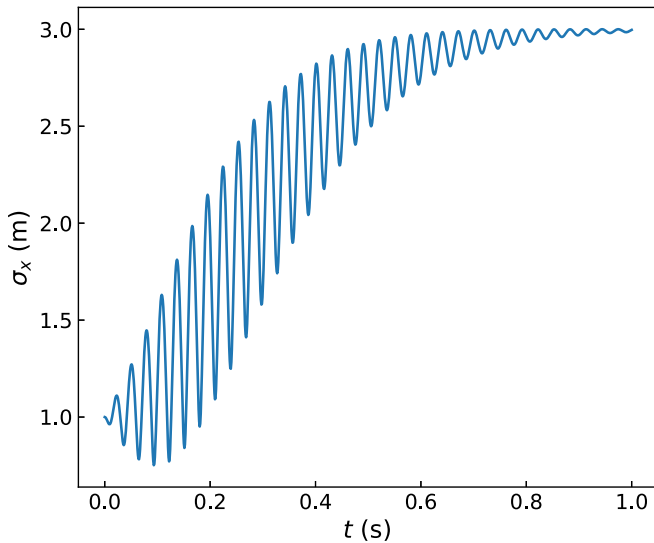

FIG. 4. The size of the cloud as a function of time, using the same parameters as Figs. 2 and 3.

terms.

$$\langle E_0 \rangle - \langle E_{\text{eq}} \rangle = \frac{3m\omega^2 \sigma_{x0}^4 \xi_D}{2x_4^2} + \frac{m\omega^2 \sigma_{x0}^4 \xi_D^2}{4x_4^2}. \quad (32)$$

These deviations are small compared to the total energy, which is proportional to $(1 + \xi_D)\sigma_x^2$. The approximations we have used all require $\xi_D \ll x_4^2$ and $\sigma_x < \sqrt{\xi_D}$, so these differences are quite small by comparison. Also notable is that the energy difference depends on the sign of x_4^2, which can be positive or negative, as described in Sec. II. For the system described and plotted in Figs. 2–4, the error is about 4%.

There is an alternative formulation for the first two moments that works for $\Lambda t \ll 1$ and converts the oscillatory part into a single cosine. For the first moment, the approximation yields

$$\langle x \rangle = \frac{\sqrt{2\xi_D}\sigma_x}{(1 + (\Lambda t)^2)^2} \exp\left[\frac{-(\Lambda t)^2 \xi_D}{1 + (\Lambda t)^2}\right]$$
$$\times \cos\left(\omega t + \phi_D + 2\Lambda t + \frac{\Lambda t \xi_D}{1 + (\Lambda t)^2}\right). \quad (33)$$

Of particular note is the argument of the cosine. The usual $\omega t + \phi_D$ is present, and there is a term proportional to ξ_D, representing the frequency dependence on the strength of the initial sloshing, but the $2\Lambda t$ term is *independent* of the kick strength. In other words, the frequency of oscillation for a cloud is different from that of a single particle, even as the oscillation amplitude approaches zero. Contrast this with Eq. (11), where the value of Ω for a single particle approaches ω as the amplitude tends to zero.

Next, the same approximation applied to Υ_{22} leads to an approximate expression for the second moment of position.

$$\langle x^2 \rangle = \sigma_x^2(1 + \xi_D) + \frac{\sigma_x^2 \xi_D}{(1 + (2\Lambda t)^2)^3} \exp\left[\frac{-(2\Lambda t)^2 \xi_D}{1 + (2\Lambda t)^2}\right]$$
$$\times \cos\left[2\omega t + 2\phi_D + 6\Lambda t + \frac{2\Lambda t \xi_D}{1 + (2\Lambda t)^2}\right]. \quad (34)$$

These two moments can similarly be combined to approximate the cloud size as a function of time.

IV. TIME OF FLIGHT

In an experimental setting, it is likely that the atomic clouds will be imaged after a period of free fall, in order to improve optical access and increase the size of the cloud and the range of its motion. In such a case, it is important to understand how the system changes during free fall and whether the time of flight drastically changes the form of the results. We will show below that the addition of time of flight increases the amplitude of oscillation of $\langle x \rangle$ and causes a phase shift, based on an approximate form for $\langle x \rangle$. We will also see that the size of the cloud changes and the envelope of oscillations in σ_x changes shape somewhat. However, the overall trends are maintained.

The evolution of the atoms in phase space in free fall can be easily understood as shearing of the phase-space density after the trap is turned off. The evolution of the center-of-mass position can be calculated by looking at the center-of-mass

position and its time derivative at the start of free fall. However, the evolution of the cloud size is difficult to express in a compact analytical form. Instead, numerical simulations are a much easier way to show this evolution, and numerical simulations can show that the behavior of the cloud after a time of flight is qualitatively similar enough that the same equations can still be used for the fit.

Time of flight affects the first moment by changing its amplitude and adding a phase shift that depends on the time of flight. Looking at the form of the first moment, Eq. (30), its general behavior is that of a sinusoid with a slowly varying amplitude. This functional form can be approximated by

$$\langle x \rangle \approx M(t)\cos(\Omega t + \phi_1), \tag{35}$$

where $M(t)$ is the decay function, Ω represents the real oscillation frequency of the cloud, and ϕ_1 represents some initial phase.

Taking the derivative of this expression, assuming that the variation of $M(t)$ is slow compared to the sinusoid, results in

$$\frac{\partial \langle x \rangle}{\partial t} \approx -\Omega M(t)\sin(\Omega t + \phi_1), \tag{36}$$

which has the same frequency of oscillation and a similar decay rate, insofar as the variation of $M(t)$ is slow, to the dynamics without time of flight. Assuming the x axis is perpendicular to gravity, the horizontal velocity of the cloud is constant after the trap is released. The result is an expression that oscillates with the same frequency, but with a different phase and amplitude that depend on the time of release and the elapsed time of flight. Since the amplitude decay function $M(t)$ carries over virtually unchanged, and since the velocity of the center of mass also decays at about the same rate, the effective value of Λ will be very similar even after time of flight.

The behavior of the cloud size is more difficult to describe analytically. Since the cloud is oscillating in a potential much larger than the cloud, the cloud may experience dispersion which can cause the cloud to expand more or less quickly after the trap is released, depending on the phase of the oscillation at the time of release. This complication makes writing a compact analytical solution, even an approximate one, to σ_x after free fall very difficult. In this case, numerical simulations are a better tool for examining the system's evolution.

Figure 5 shows the results of a numerical model for the behavior of $\langle x \rangle$ and σ_x, in conditions chosen to be similar to the parameters used in Figs. 2–4. Fourth-order Runge-Kutta integration was used to produce the results. We observe that the behavior with and without time of flight are similar but the time-of-flight data has a larger amplitude of oscillation and a larger cloud size in general. The time of flight exaggerates the oscillations in σ_x, changing the shape of the curve, with more exaggerated size oscillations at intermediate times. However, the shapes of the two curves are very similar to our analytical solution, so it should be possible to fit the same parameters to the time-of-flight data and reach similar conclusions. For example, it should still be possible to fit Λ to the data and minimize it in order to achieve a maximally harmonic trap, though the values for Λ in time of flight may be slightly different than if observed without time of flight. The overall trends are preserved.
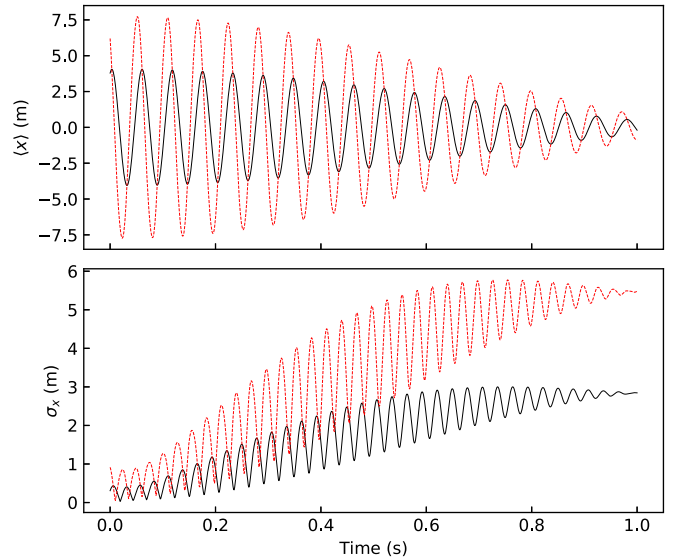

FIG. 5. Pictured here are the results of a Monte Carlo numerical simulation of sloshing in a harmonic plus quartic trap. Along the vertical axis, the top subplot describes the center-of-mass position of the cloud and the bottom subplot shows the cloud size. The horizontal axis in both subplots describes how long the cloud was allowed to slosh in the trap before turning off the trapping potential for time of flight. The black curves represent the position and size of the cloud without time of flight. The dotted curves (red online) show the position and size of the cloud after a time of flight of 0.015 s. The other simulation parameters are $m = 1$ kg, $\omega = 100$ s^{-1}, and $x_4 = 8$ m. The value of $k_B T$ is 10000 J. The clouds were generated in a harmonic potential, then given a kick by introducing a gradient of $-2.4x$ J/m for 0.021 s. These values were chosen to make the results without time of flight similar to the results in Figs. 2–4, in order to ease comparison between the analytical solution and the simulation.

V. CONCLUSIONS AND OUTLOOK

The oscillations along the weak axis of a small cloud in a perfectly harmonic cigar-shaped trap are not expected to decay significantly over time, based on a straightforward extension of the calculations in Guéry-Odelin *et al.* [22]. The addition of nonharmonic terms causes the cloud to gradually spread out and reach a state that looks like equilibrium even without interactions, as atoms with different energies gradually drift apart.

Our analytical model describes the dynamics of a classical cloud of noninteracting particles in a harmonic trap with a quartic perturbation. We make some minor approximations and assumptions about the initial conditions and single-particle dynamics. With these few conditions, the system is analytically solvable. The analytical expressions can be used as fitting functions for the observed behavior of ensembles of cold atoms in a harmonic plus quartic trap, even after a short time of flight. The motion of the ensemble's center of mass and the evolution of its size permit easy determination of trap anharmonicity, and, given the right architecture, the anharmonic parts can be tuned to some desired value by observing the value of Λ. Minimizing Λ results in a maximally harmonic trap, and if some specific quartic contribution is desired, Λ can be used to approach that value.

Time-of-flight imaging makes small changes to the observed values of the variables but does not qualitatively change the behavior of the ensemble. Even with time-of-flight imaging, the fit parameters for the trap still maintain the same relative trends.

The construction of a trap geometry which can control various polynomial terms while minimizing unwanted terms is discussed in Stickney *et al.* [17]. The specific calculations for a trap allowing adjustment of harmonic and quartic terms, while canceling polynomial terms out to sixth order are also detailed there. Experimental realization of such an atom chip trap is expected to lead to measured dynamics similar to our analytical model, and may be worth exploring. Dynamic control of the shape of the trap is expected to produce additional interesting results. For instance, because the equilibrium is deterministic and not a true thermal equilibrium, it should be possible to reverse the apparent equilibration of the cloud somewhat by changing the sign of the quartic perturbation as long as the collision rate is not too high, and it may even be possible to engineer "pauses" in the apparent equilibration by turning off the quartic contributions. These qualities make the dynamically controlled trap an additional interesting topic worthy of experimental examination.

ACKNOWLEDGMENTS

[1] J. B. Fixler, G. T. Foster, J. M. McGuirk, and M. A. Kasevich, Science **315**, 74 (2007).

[2] A. Peters, K. Y. Chung, and S. Chu, Metrologia **38**, 25 (2001).

[3] A. Bertoldi, G. Lamporesi, L. Cacciapuoti, M. de Angelis, M. Fattori, T. Petelski, A. Peters, M. Prevedelli, J. Stuhler, and G. M. Tino, Eur. Phys. J. D **40**, 271 (2006).

[4] V. Xu, M. Jaffe, C. D. Panda, S. L. Kristensen, L. W. Clark, and H. Müller, Science **366**, 745 (2019).

[5] B. Canuel, F. Leduc, D. Holleville, A. Gauguet, J. Fils, A. Virdis, A. Clairon, N. Dimarcq, C. J. Bordé, A. Landragin, and P. Bouyer, Phys. Rev. Lett. **97**, 010402 (2006).

[6] X. Wu, F. Zi, J. Dudley, R. J. Bilotta, P. Canoza, and H. Müller, Optica **4**, 1545 (2017).

[7] S. M. Dickerson, J. M. Hogan, A. Sugarbaker, D. M. S. Johnson, and M. A. Kasevich, Phys. Rev. Lett. **111**, 083001 (2013).

[8] J. H. T. Burke and C. A. Sackett, Phys. Rev. A **80**, 061603(R) (2009).

[9] S. Wu, E. J. Su, and M. G. Prentiss, Phys. Rev. Lett. **99**, 173201 (2007).

[10] I. Dutta, D. Savoie, B. Fang, B. Venon, C. L. Garrido Alzar, R. Geiger, and A. Landragin, Phys. Rev. Lett. **116**, 183003 (2016).

[11] B. Deissler, K. J. Hughes, J. H. T. Burke, and C. A. Sackett, Phys. Rev. A **77**, 031604(R) (2008).

[12] R. Bouchendira, P. Cladé, S. Guellati-Khélifa, F. Nez, and F. Biraben, Phys. Rev. Lett. **106**, 080801 (2011).

[13] K. Y. Chung, S. W. Chiow, S. Herrmann, S. Chu, and H. Müller, Phys. Rev. D **80**, 016002 (2009).

[14] J. A. Stickney, D. Z. Anderson, and A. A. Zozulya, Phys. Rev. A **75**, 063603 (2007).

[15] M. Horikoshi and K. Nakagawa, Phys. Rev. Lett. **99**, 180401 (2007).

[16] R. P. Kafle, D. Z. Anderson, and A. A. Zozulya, Phys. Rev. A **84**, 033639 (2011).

[17] J. A. Stickney, E. Imhof, B. Kasch, B. R. Kroese, J. A. R. Crow, S. E. Olson, and M. B. Squires, Phys. Rev. A **96**, 053606 (2017).

[18] T. Berrada, S. van Frank, R. Bücker, T. Schumm, J.-F. Schaff, and J. Schmiedmayer, Nat. Commun. **4**, 2077 (2013).

[19] U. Delić, D. Grass, M. Reisenbauer, T. Damm, M. Weitz, N. Kiesel, and M. Aspelmeyer, Quantum Sci. Technol. **5**, 025006 (2020).

[20] J. Gieseler, L. Novotny, and R. Quidant, Nat. Phys. **9**, 806 (2013).

[21] T. Weiss and O. Romero-Isart, Phys. Rev. Research **1**, 033157 (2019).

[22] D. Guéry-Odelin, F. Zambelli, J. Dalibard, and S. Stringari, Phys. Rev. A **60**, 4851 (1999).

[23] D. S. Lobser, A. E. S. Barentine, E. A. Cornell, and H. J. Lewandowski, Nat. Phys. **11**, 1009 (2015).

[24] J. A. Stickney, M. B. Squires, J. Scoville, P. Baker, and S. Miller, Phys. Rev. A **79**, 013618 (2009).

[25] I. S. Gradshteyn and I. M. Ryzhik, *Table of Integrals, Series, and Products*, 7th ed. (Elsevier/Academic Press, Amsterdam, 2007); translated from the Russian (translation edited and with a preface by Alan Jeffrey and Daniel Zwillinger).